Inorganic Chemistry

Article

pubs.acs.org/IC

pH and Ligand Dependent Assembly of Well−Dawson Arsenomolybdate Capped Architectures

He Zhang,[†,‡] Kai Yu,*[,†,‡] Chunmei Wang,[†,‡] Zhanhua Su,[†,‡] Chunxiao Wang,[†,‡] Di Sun,[§] Honghong Cai,[†,‡] Zhaoyi Chen,[†,‡] and Baibin Zhou*[,†,‡]

[†]Key Laboratory for Photonic and Electronic Bandgap Materials, Ministry of Education, School of Chemistry annd Chemical Enginerring, Harbin Normal University, No.1 South of shida Road Limin Development Zone, Harbin City Helongjiang Province, Harbin 150025, China

[‡]Key Laboratory of Synthesis of Functional Materials and Green Catalysis, Colleges of Heilongjiang Province, Harbin Normal University, Harbin 150025, China

[§]School of Chemistry and Chemical Engineering, Shandong University, Jinan 250100, China

Supporting Information

ABSTRACT: Five Well−Dawson-type arsenomolybdates, formulated as $[Cu(2,2'\text{-bpy})_2][\{Cu(2,2'\text{-bpy})\}_3\{As_2^{V}Mo_2^{V}Mo_{16}^{VI}O_{62}\}]\cdot 4H_2O$ (**1**), $[H_2(4,4'\text{-bpy})]_{2.5}[As^{III}(As_2^{V}Mo_2^{V}Mo_{16}^{VI}O_{62})]\cdot 5H_2O$ (**2**), $(pyr)(imi)(Himi)_3[As_2^{III}(As_2^{V}Mo_3^{V}Mo_{15}^{VI}O_{62})]\cdot 3H_2O$ (**3**), $[As_3^{III}(As_2^{V}Mo_3^{V}Mo_{15}^{VI}O_{62})]\cdot 4H_2O$ (**4**), and $(H_2btp)_3[As_2^{V}Mo_{18}^{VI}O_{62}]\cdot 6H_2O$ (**5**) (bpy = bipyridine, pyr = pyrazine, imi = imidazole, btp = 1,5-bis(triazol)pentane), have been hydrothermally synthesized and structurally characterized by the elemental analysis, TG, IR, UV−vis−NIR, XPS, XRD, and single-crystal X-ray diffraction. The structural analysis indicates that compounds **1**−**4** contain rare reduced Dawson $\{As_2Mo_{18}O_{62}\}$ (abbreviated as $\{As_2Mo_{18}\}$) anions as parent cluster unit, which are capped by a certain number of Cu(II) or As(III) species on different coordination positions via altering pH values and organic ligand of the reaction system. Compounds **1** and **2** are asymmetric tricopper and monoarsenate(III) capped assemble by three $\{Cu(bpy)\}^{2+}$ and a $\{AsO_3\}$ fragments, respectively. Compounds **3** and **4** are symmetric biarsenate(III) and triarsenate(III) capped cluster by four and six half occupancy $\{AsO_3\}$ units, respectively. Compound **5** is uncapped $\{As_2Mo_{18}\}$ structures. Compounds **1**−**4** represent infrequent Dawson arsenomolybdate capped architectures, especially **2**−**4**, as arsenate(III) capped Dawson-type assemblies are observed for the first time. Compounds **1**−**5** display good electrocatalytic activity on reduction of nitrite. Compounds **1**, **2**, **3**, and **5** exhibit fluorescent properties in the solid state at room temperature. In addition, magnetic properties of **1**−**4** have been investigated in detail.

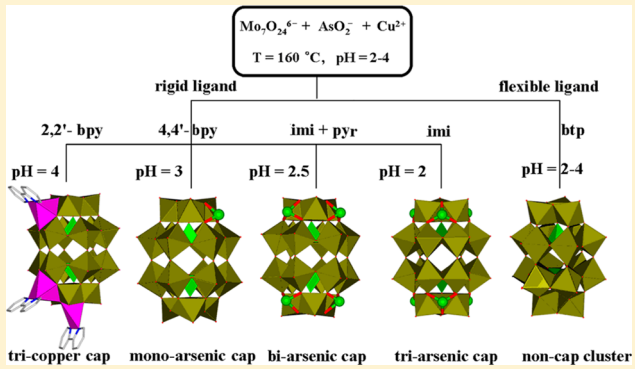

INTRODUCTION

Polyoxometalates (POMs) have attracted great interest due to their structural variety and desirable properties, which endow them with potential applications in catalysis,[1] gas storage and adsorption,[2] electromagnetic functional materials,[3] biomedicine,[4] and photochemistry.[5] The Wells−Dawson cluster was first synthesized by Wells in 1945, and determined by Dawson in 1953. Since then, the conventional Dawson-type structures $[M_{18}O_{54}(XO_4)_2]^{n-}$ (M = Mo, W, and X = P, As, S, or I) become the most widely recognized POM anion and have been intensively studied in structures and applications. However, compared with classical Keggin POM compounds, the related reports on the saturated Dawson-type anions are much less common for their larger steric hindrances and lower electron density of surface. Nowadays, the development of Dawson-type POMs is mostly dependent on the synthesis of compounds holding new structures and properties. The hydrothermal synthesis techniques in combination with the organic templates have been demonstrated to be a popular strategy in the isolation of such materials. Up to now, a large number of POM-based hybrids have been assembled successfully through $[P_2W_{18}O_{62}]^{n-}$ clusters incorporating multiple transition-metal ions or metal−organic units leading to a growing family of transition-metal substituted polytungstates.[6] Compared with abundant heteropolytungstates, the heteropolymolybdate (HPM) analogues are very limited for unstable polymolybdate precursors. In particular, research on analogues containing arsenic as heteroatom HPMs has been far unexplored, and only four $\{As_2Mo_{18}\}$-based compounds have been reported.[7] In fact, Dawson arsenomolybdate will show a great variety of properties owing to the redox active nature of both molybdenum and

Received: June 23, 2014
Published: November 14, 2014

   dx.doi.org/10.1021/ic5014973 | Inorg. Chem. 2014, 53, 12337−12347

arsenic. Thus, it is interesting and challenging to change the inner $\{XO_4\}$ units of the Dawson POMs with arsenic elements, especially considering that such exchange can lead to new POM species with unprecedented properties that arise from the intramolecular electronic interactions between the encapsulated anions and the Dawson metal-oxide cages. On the other hand, in most self-assembly reactions for arsenomolybdate, As_2O_3 is usually used as As^{III}-containing raw material,[8] which can provide different coordination geometries (tetrahedron for the As^V element, triangular pyramid for the As^{III} element) incorporating into the polyoxoanion backbones in the form of the arsenomolybdate because As_2O_3 is inclined to be partially oxidized to As^V in reactions. However, their highly toxic property has always been a formidable drawback. In this sense, further research on introducing arsenic elements into Dawson core utilizing low toxic arsenic salts as raw material is necessary and meaningful in this branch.

In contrast to greater attention having been paid to the selection of metal−ligand fragments for hybrids, the surface modification of the POM cluster itself adjusting to anionic structures and properties is limited relatively. The introduction of hydrothermal technique has also led to the appearance of various inorganic capped POM-type assemblies. Metal or nonmetallic elements may be grafted to the surface of the POM through bridging and terminal oxygen atoms to form various capped derivatives by this method, which also achieve the purpose of adjusting POM structures and properties. Recently, a number of POMs with the capping groups have been reported, such as bi-, tri-, tetra-, and hexacapped structures.[9] The capping groups in these derivatives are mainly restricted to high oxidation state metals (V) and divalent transition metals (Ni and Cu). In some cases, the rare-earth ions,[10] alcohol organic ligand,[11] selenium,[12] antimony,[13] and boron[14] are also found to be a cap unit on the POM cluster, which greatly enriched the kinds of POMs. Among these reported works, only a small POM cluster unit, such as Mo_4O_{13}, Mo_5O_{15}, or Anderson structures, can be further capped by AsO_4, $RAsO_3$, PO_4, RPO_3, and SO_4.[15] However, studies on POM with capping XO_3 groups (X = Se^{IV}, As^{III}, and Sb^{III}) are rare.[16] Significantly, arsenic usually adopts triangular pyramid coordination geometries for As^{III}, which not only can be encapsulated to the POMs skeletons acting as the heteroatoms[6] but also can be grafted to the surface of the POM to form capped POM species.[17] Nevertheless, studies on large polymolybdates with capping AsO_3 groups are really rare. Recently, Niu et al. addressed a series of arsenomolybdate architectures constructed from a monoarsenic capped trivacant $[As^{III}As^{V}Mo_9O_{34}]^{6-}$ anion.[8] Inspired by the excellent work described above, we expect to introduce $\{AsO_3\}$ cap to a conventional Dawson cluster with the aim of developing a novel POM system. On the other hand, less attention has been paid to investigating the relationship between the structure of POM capped assemblies and the external physical or chemical stimuli, despite the external stimuli having been demonstrated as playing a key role in the control of the number, position, and types of cap. All the contexts provide us a large opportunity to explore Well−Dawson arsenatomolybdate capped architectures.

In this Article, a certain number of Cu^{2+} or As^{3+} were introduced into Well−Dawson $\{As_2Mo_{18}\}$ system to act as cap by hydrothermal reaction of $NaAsO_2$ as raw material, which lead to five novel arsenomolybdate, namely, $[Cu(2,2'\text{-bpy})_2][\{Cu(2,2'\text{-bpy})\}_3\{As_2^{V}Mo_2^{V}Mo_{16}^{VI}O_{62}\}]\cdot 4H_2O$ (**1**), $[H_2(4,4'\text{-bpy})]_{2.5}[As^{III}(As_2^{V}Mo_2^{V}Mo_{16}^{VI}O_{62})]\cdot 5H_2O$ (**2**), $(pyr)(imi)(Himi)_3[As_2^{III}(As_2^{V}Mo_3^{V}Mo_{15}^{VI}O_{62})]\cdot 3H_2O$ (**3**), $[As_3^{III}(As_2^{V}Mo_3^{V}Mo_{15}^{VI}O_{62})]\cdot 4H_2O$ (**4**), and $(H_2btp)_3[As_2^{V}Mo_{18}^{VI}O_{62}]\cdot 6H_2O$ (**5**). Our result further suggests that the kind, number, and location of cap may be controlled by altering pH and organic ligand of the reaction system.

EXPERIMENTAL SECTION

General Methods and Materials. All chemicals were commercially purchased and used without further purification. Elemental analyses (C, H, and N) were performed on a PerkinElmer 2400 CHN elemental analyzer; As, Mo, and Cu were analyzed on a PLASMA-SPEC (I) ICP atomic emission spectrometer. The IR spectrum was recorded in the range 400−4000 cm^{-1} on an Alpha Centaurt FT/IR spectrophotometer using KBr pellets. The UV−vis−NIR absorption spectroscopy was measured with a Varian Cary 500 UV−vis−NIR spectrometer. X-ray photoelectron spectrum (XPS) analyses were performed on a VG ESCALAB MK II spectrometer with a Mg Kα (1253.6 eV) achromatic X-ray source. XRD patterns were collected on a Rigaku Dmax 2000 X-ray diffractometer with graphite monochromatized Cu Kα radiation (λ = 0.154 nm) and 2θ ranging from 5° to 50°. TG analyses were performed on a Perkin−Elmer TGA7 instrument in flowing N_2 with a heating rate 10 °C min^{-1}. The electrochemical measurement was carried out on a CHI 660 electrochemical workstation at room temperature (25−30 °C). A conventional three-electrode system was used. The working electrode was a carbon paste electrode (CPE), a Pt wire was the counter electrode, and Ag/AgCl (3 M KCl) electrode was used as a reference electrode. Fluorescence spectra were performed on a Hitachi F-4500 fluorescence/phosphorescence spectrophotometer with a 450 W xenon lamp as the excitation source. Magnetic susceptibility data were collected over the temperature range 2−300 K in a magnetic field of 1000 Oe on a Quantum Design MPMS-5 SQUID magnetometer.

Syntheses of $[Cu(2,2'\text{-bpy})_2][\{Cu(2,2'\text{-bpy})\}_3\{As_2^{V}Mo_2^{V}Mo_{16}^{VI}O_{62}\}]\cdot 4H_2O$ (1). The mixture of $(NH_4)_6Mo_7O_{24}\cdot H_2O$ (1.181g, 1.00 mmol), $NaAsO_2$ (0.389g, 3.00 mmol), 2,2-bipyridine (0.312 g, 2.00 mmol), and H_2O (18 mL, 1.0 mol), with or without the presence of $CuCl_2\cdot 2H_2O$, was stirred for half an hour. The pH value was adjusted to about 4.0 with 1 M HCl. The above mixture was sealed in a 25 mL Teflon reactor and heated at 160 °C for 5 days. Dark blue block crystals of **1** were isolated. The crystalline products were collected by filtration, washed with distilled water, and air-dried to give a yield of 42% (based on Mo). Anal. Calcd for $C_{50}H_{48}As_2Cu_4Mo_{18}N_{10}O_{66}$ (M_r = 3975.95): C, 15.09; H, 1.21; N, 3.52; As, 3.77; Cu, 6.44; Mo, 43.43. Found: C, 15.07; H, 1.24; N, 3.49; As, 3.80; Cu, 36.41; Mo, 43.46. IR (KBr pellet, cm^{-1}): 3256 (br), 1654 (s), 1508 (m), 992 (s), 902 (s), 834 (s), 756 (s) .

Synthesis of $[H_2(4,4'\text{-bpy})]_{2.5}[As^{III}(As_2^{V}Mo_2^{V}Mo_{16}^{VI}O_{62})]\cdot 5H_2O$ (2). Compound **2** was prepared with a method similar to that of compound **1**, except that the initial chemical 2,2-bipyridine was substituted by 4,4-bipyridine (0.312 g, 2.00 mmol), and the pH value of solution was adjusted to about 3.0 with 1 M HCl. Dark blue block crystals of **2** were isolated. The crystalline products were collected by filtration, washed with distilled water, and air-dried to give a yield of 42% (based on Mo). Anal. Calcd for $C_{25}H_{30}As_3Mo_{18}N_5O_{67}$ (M_r = 3424.22): C, 8.76; H, 0.88; N, 2.04; As, 6.56; Mo, 50.43. Found: C, 8.73; H, 0.91; N, 2.01; As, 6.59; Mo, 50.42. IR (KBr pellet, cm-1): 3265 (br), 1637 (s), 1416 (s), 989 (s), 904 (s), 813 (s), 749 (s) .

Synthesis of $(pyr)(imi)(Himi)_3[As_2^{III}(As_2^{V}Mo_3^{V}Mo_{15}^{VI}O_{62})]\cdot 3H_2O$ (3). Compound **3** was prepared with a method similar to that of compound **1**, except that the initial chemical 2,2-bipyridine was substituted by imi (0.136g, 2.00 mmol) and pyr (0.162g, 2.00 mmol), and the pH value of solution was adjusted to about 2.5 with 1 M HCl. Dark blue block crystals of **3** were isolated. The crystalline products were collected by filtration, washed with distilled water, and air-dried to give a yield of 48% (based on Mo). Anal. Calcd for $C_{16}H_{22}As_4Mo_{18}N_{10}O_{65}$ (M_r = 3421.04): C, 5.61; H, 0.64; N, 4.09; As, 8.76; Mo, 50.48. Found: C, 5.59; H, 0.66; N, 4.06; As, 8.78; Mo, 50.47. IR (KBr pellet, cm-1): 3254 (br), 1630 (s), 1505 (m), 990 (s), 918 (s), 826 (s), 745 (s) .

dx.doi.org/10.1021/ic5014973 | Inorg. Chem. 2014, 53, 12337−12347

Table 1. X-ray Crystallographic Data for 1−5

	1	2	3	4	5
formula	$C_{50}H_{48}As_2Cu_4Mo_{18}N_{10}O_{66}$	$C_{25}H_{30}As_3Mo_{18}N_5O_{67}$	$C_{16}H_{22}As_4Mo_{18}N_{10}O_{65}$	$As_5H_{10}Mo_{18}O_{67}$	$C_{27}H_{54}As_2Mo_{18}N_{18}O_{68}$
fw (g mol^{-1})	3975.95	3424.22	3421.04	3183.60	3595.64
cryst syst	monoclinic	triclinic	orthorhombic	monoclinic	triclinic
space group	$C2/m$	$P\bar{1}$	$Pmmn$	$P2_1/m$	$P\bar{1}$
a (Å)	26.789(5)	13.647(5)	19.627(3)	13.770(6)	13.1740(5)
b (Å)	18.835(3)	14.141(5)	13.5679(19)	19.780(8)	16.4284(7)
c (Å)	20.356(4)	24.136(9)	13.9399(18)	14.006(6)	21.4212(9)
α (deg)	90.00	78.485(4)	90.00	90.00	80.6570(10)
β (deg)	106.847(3)	81.140(4)	90.00	111.572(7)	83.9260(10)
γ (deg)	90.00	65.260(4)	90.00	90.00	69.03
V (Å)	9830(3)	4132(3)	3712.2(9)	3548(2)	4265.9(3)
Z	4	2	2	2	2
d_{calcd} (Mg cm^{-3})	2.687	2.752	3.061	2.980	2.799
μ (mm^{-1})	3.829	3.932	4.816	5.484	3.439
GOF on F^2	1.042	1.097	1.082	1.256	1.012
final R indices[a] $[I > 2\sigma(I)]$	R1 = 0.0573, wR2 = 0.0914	R1 = 0.0873, wR2 = 0.1018	R1 = 0.0637, wR2 = 0.0974	R1 = 0.0587, wR2 = 0.0969	R1 = 0.0351, wR2 = 0.0810

[a] $R1 = \sum||F_o| - |F_c||/\sum|F_o|$. $wR2 = \{R_w[(F_o)^2 - (F_c)^2]^2/R_w[(F_o)^2]^2\}^{1/2}$.

Synthesis of $[As_3^{III}(As_2^{V}Mo_3^{V}Mo_{15}^{VI}O_{62})]\cdot 4H_2O$ (4). Compound **4** was prepared with a method similar to that of compound **1**, except that the initial chemical 2,2-bipyridine was substituted by imi (0.136g, 2.00 mmol), and the pH value of solution was adjusted to about 2.0 with 1 M HCl. Dark blue block crystals of **4** were isolated. The crystalline products were collected by filtration, washed with distilled water, and air-dried to give a yield of 56% (based on Mo). Anal. Calcd for $As_5H_{10}Mo_{18}O_{67}$ (M_r = 3183.60): As, 11.77; H, 0.32; Mo, 54.24. Found: As, 11.81; H, 0.28; Mo, 54.29. IR (KBr pellet, cm-1): 3250 (br), 1623 (s), 985 (s), 875 (s), 750 (s).

Synthesis of $(H_2btp)_3[As_2^{V}Mo_{18}^{VI}O_{62}]\cdot 6H_2O$ (5). Compound **5** was prepared with a method similar to that of compound **1**, except that the initial chemical 2,2-bipyridine was substituted by 1,5-bis(triazol)-pentane (0.206 g, 1.00 mmol), and the pH value of the solution was adjusted to about 3.5 with 1 M HCl. Dark green crystals of **5** were isolated. The crystalline products were collected by filtration, washed with distilled water, and air-dried to give a yield of 42% (based on Mo). Anal. Calcd for $C_{27}H_{54}As_2Mo_{18}N_{18}O_{68}$ (M_r = 3595.64): C, 9.01; H, 1.50; N, 7.01; As, 8.33; Mo, 48.03. Found: C, 9.03; H, 1.48; N, 7.05; As, 8.31; Mo, 48.01. IR (KBr pellet, cm-1): 3432 (br), 1653 (s), 1469 (m), 986 (s), 832 (s), 764 (s), 685 (s).

X-ray Crystallography. Single crystal was mounted on a glass fiber, and the data were collected at 293 K on a Bruker SMART CCD diffractometer with graphite-monochromated Mo Kα radiation (λ = 0.710 73 Å). Semiempirical absorption correction based on symmetry equivalent reflections was applied. The structure was solved by direct methods and refined by the full-matrix least-squares method based on F^2. Structure solution, refinement, and generation of publication materials were performed with the use of the SHELXTL crystallographic software package.[18] All of the non-hydrogen atoms were refined anisotropically. Hydrogen atoms on carbon atoms of organic ligands were included at calculated positions and refined with a riding model. The H atoms on water molecules were not included and just put into the final molecular formula. A summary of crystal data and structure refinement for compounds **1**−**5** was provided in Table 1. Selected bond lengths and angles for compound **1**−**5** are listed in Supporting Information Table S1. Crystallographic data for the structures have been deposited in the Cambridge Crystallographic Data Centre with CCDC 983688 for **1**, 983689 for **2**, 983690 for **3**, 983691 for **4**, and 991507 for **5** contain the supplementary crystallographic data for this Article. These data can be obtained free of charge from the Cambridge Crystallographic Data Centre via www.ccdc.cam.ac.uk/data_request/cif.

RESULTS AND DISCUSSION

Synthesis. Owing to the lability and instability of $\{As_2Mo_{18}\}$ in the solution, it is very difficult to prepare and isolate Dawson arsenomolybdate precursors. During our research on the exploration of capped arsenomolybdate species, hydrothermal reaction of simple raw materials was employed. The reactions of $(NH_4)_6Mo_7O_{24}\cdot H_2O$, $NaAsO_2$, and $CuCl_2\cdot 2H_2O$ with almost equal stoichiometry in the presence of different organic ligands have been investigated. Compounds **1**−**5** were synthesized by altering pH values of the reaction system. At the beginning, when 2,2′-bpy was added at the pH of 4.0, compound **1** (a tricapped hybrid by three {Cu(bpy)} fragments through bridging oxygen atoms on "polar" and "equator" position) was prepared. When 2,2′-bpy was replaced by 4,4′-bpy and the pH value was decreased to 3.0, compound **2** (asymmetric monocapped assemble modified by a $\{AsO_3\}$ fragments via μ-O atoms on one side of $\{Mo_3O_{13}\}$ unit) was obtained. When organic ligand was replaced by imidazole and pyridine, the pH values decreased to 2.5, and compound **3** (symmetric bicapped structure decorated by four half occupy As(III) on four symmetric position of both side of $\{Mo_3O_{13}\}$ unit) was obtained. When the ligand was replaced by imi, with the pH value at a low level (pH = 2.0), compound **4** (another symmetric tricapped cluster capped by six disorder $\{AsO_3\}$ segment via μ-O atoms on six symmetric position of both side of $\{Mo_3O_{13}\}$ unit) was formed. Parallel experiments reveal that the pH value of the {Cu/As/Mo} system varying in the range 3.8−4.2 favors the formation of copper capped Dawson structure **1**; the lower pH of 3.0−2.0 trends to the formation of arsenate capped cluster. Furthermore, more arsenate(III) caps are implanted in more "polar" position of Dawson skeleton under lower pH value, which is possibly because the organic ligands tend to be protonated at lower pH value (2.0−3.0), and fail to bond to the copper ions. Meanwhile, more bridging oxygen atoms on "polar" position are inclined to be further activated. It is clear that acidity of the solution is the key factor influencing the kind, number, and locations of cap for these compounds. Besides, capped compounds **1**−**4** are formed in the presence of different rigid organic ligands. While flexible ligand btp was introduced to the reaction system, 0D

dx.doi.org/10.1021/ic5014973 | Inorg. Chem. 2014, 53, 12337−12347

arsenomolybdate clusters without cap can be obtained under a wide pH range from 4 to 2. This indicates that flexible ligands are more likely to be protonated than rigid ligands, which is not conducive to the formation of the cap. It is unsuccessful for all of our attempts to use one of the above ligands to induce compounds **1**−**5**, which shows that the kind of organic ligand affects the formation of these compounds. In addition, Dawson crystals were found to be sensitive to reaction time and temperature, which were controlled strictly to be 5 days and reaction temperature 160 °C. With reaction time beyond 5 days under the similar hydrothermal treatment of **4**, another arsenomolybdate $[\{Cu(imi)_2\}_3As_3Mo_3O_{15}]\cdot H_2O$ was obtained.[19a] If the reaction temperature is lower than 160 °C for **4**, a bicapped Anderson structure $[Cu(imi)_2]_2[\{(CuO_6)(As_3O_3)_2Mo_6O_{18}\}\{Cu(imi)_2\}_2]$ was obtained.[19b] No crystals could be obtained outside the time and temperature ranges for the other four reactions. It is worth noting that controlling the molar ratio of $(NH_4)_6Mo_7O_{24}\cdot H_2O$ and $NaAsO_2$ at 1:3 favors the isolation of high-quality crystals. Here, we further explore the influence of different transition-metal cations by using $FeCl_3$, $NiCl_2$, $MnCl_2$, $CoCl_2$, etc., to replace $CuCl_2$ or absent TM cations under the similar hydrothermal treatment of **2**−**4**. Curiously, compounds **2**−**4** can still be formed under the above context, which indicates that TM cations do not have influence on the structural configurations of arsenate capped clusters under similar conditions in our case. It also means that the arsenic capped clusters are inert and difficult to substitute further by transition-metal complexes in our system. The formations of these complexes are shown in Scheme 1.

Scheme 1. Illustration of the Relationship between Capped Structures of Dawson-type Arsenomolybdate and Different pH and/or Organic Ligands

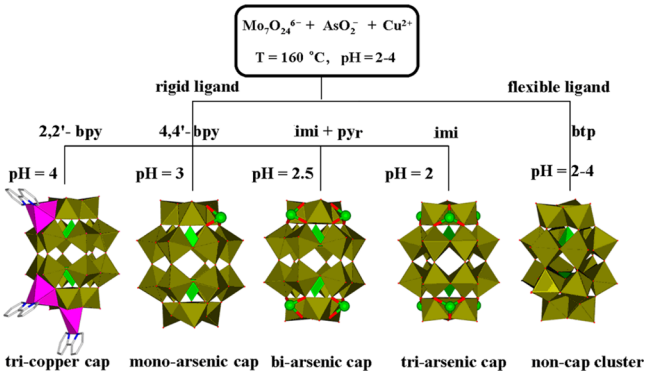

Although rare Dawson arsenomolybdates exhibiting interesting cap structure are formed via adjusting pH values and organic ligand of the reaction system, the synthesis and exploration of high-dimensional covalent organic−inorganic hybrids based on these cap structures still remains a great challenge to us

Structure Description. Single-crystal X-ray diffraction analysis reveals that compounds **1**−**5** contain a Well−Dawson $\{As_2Mo_{18}\}$ cluster as parent cluster unit, which consists of two $[\alpha\text{-A-}AsMo_9O_{34}]^{9-}$ units derived from α-Keggin anion by removal of a set of three corner-shared MoO_6 octahedra. Its Mo−O distances can be grouped into three sets: Mo−Ot (terminal) 1.666(10)−1.735(3) Å, Mo−Ob (bridge) 1.863(11)−1.985(3) Å, and Mo−Oc (central) 2.272(3)−2.411(7) Å. The central As atoms exhibit tetrahedral coordination modes with the As−O bond lengths in the range 1.518(9)−1.590(8) Å. The As−O bond lengths and O−As−O bond angles are in the normal ranges.

Bond valence sum (BVS) calculations[20] show average values of ca. 5.87, 5.89, 5.83, and 5.82 for Mo centers in **1**, **2**, **3**, and **4**, respectively, which is close to the result of 16 Mo^{6+} and 2 Mo^{5+} in **1** and **2**, and 15 Mo^{6+} and 3 Mo^{5+} in **3** and **4**, respectively. BVS results are approximately 5.96−6.02 for Mo centers in **5**, indicating that their oxidation states are +VI oxidation states. BVS calculations for all the As atoms in **1**−**5** illustrate that the oxidation states of four-coordinate As and three-coordinate As elements are +5 and +3, respectively. These results are in good agreement with their usual geometric configurations. Notably, only $NaAsO_2$ was used as the starting material; however, the As^V element was observed in the products. Therefore, part of $NaAsO_2$ reactants must have been oxidized in the reaction. A similar phenomenon can be observed in previous literature reports.[8] BVS calculations also confirm that all Cu atoms in **1** are in +II oxidation states. Moreover, one or two extra protons should be added to the organic ligand bpy in **2**, imi in **3**, and btp in **5** for the charge balance. Thus, compounds **1**−**5** can be formulated as mentioned above.

Structure of $[Cu(2,2'\text{-bpy})_2][\{Cu(2,2'\text{-bpy})\}_3\{As_2^VMo_2^VMo_{16}^{VI}O_{62}\}]\cdot 4H_2O$ (1). Compound **1** consists of one $[\{Cu(2,2'\text{-bpy})\}_3\{As_2^VMo_2^VMo_{16}^{VI}O_{62}\}]^{2-}$, one $\{Cu((2,2'\text{-bpy})_2\}$ counterion, and four lattice water molecules (Supporting Information Figure S1). The basic unit $\{As_2Mo_2^V Mo_{16}^{VI}O_{62}\}^{8-}$ is a reduced Dawson heteropolyanion. The BVS calculation shows that 2 out of 18 Mo atoms are in +5 oxidation states with 2 electrons delocalized within the whole metal−oxide cluster. An unusual structural feature of compound **1** is that the surface bridging oxygen atoms of the Dawson polyoxoanion are coordinated to three $\{Cu(2,2'\text{-bipy})\}^{2+}$ fragments. There are four crystallographically independent copper atoms (Cu1, Cu2, Cu3, and Cu4), which exhibit three kinds of coordination geometries coexisting in the structure **1** (Figure 1). As for Cu2 and Cu3, they exhibit

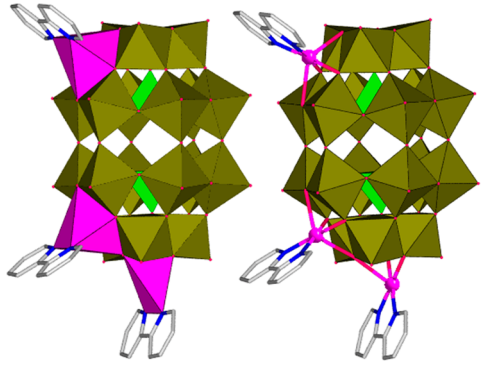

Figure 1. Tricopper capped Dawson arsenomolybdate and the coordination environment of Cu-cap in **1**.

octahedral coordination environment with three μ-O atoms of "polar" positions, one μ-O atoms of "equator" positions, and two nitrogen atoms from one 2,2′-bipy ligand. In this linkage mode, two $\{Cu(2,2'\text{-bipy})\}$ complexes are implanted in two symmetrical pits between "polar" and "equator" positions of one side of $\{As_2Mo_{18}\}$ units. The Cu1 atom is pentacoordinated by three μ-O atoms of "polar" positions and two nitrogen atoms from one 2,2′-bipy ligand. In this way, another $\{Cu(2,2'\text{-bipy})\}$ complex is grafted on $\{Mo_3O_{13}\}$ "polar" faces of $\{As_2Mo_{18}\}$ units. The Cu4 displays a distorted tetrahedral

dx.doi.org/10.1021/ic5014973 | Inorg. Chem. 2014, 53, 12337−12347

coordination environment, which is defined by four nitrogen atoms from two 2,2′-bipy ligands. The Cu−O and Cu−N distances are in the ranges 1.961(10)−2.409(15) and 1.982(11)−2.012(13) Å, respectively. The adjacent polyoxoanion clusters are aggregated together via supramolecular interactions between C atoms of $\{Cu(2)(2,2'\text{-bpy})_3\}$ fragments and terminal O atoms of Dawson-type anion to form dimeric cluster with (O16···C23 3.033 Å, O16···C24 3.138 Å, Supporting Information Figure S2a). The adjacent dimeric units are bonded together to form infinite 1D dimeric chains via the $\pi-\pi$ interactions with the average distance between two 2,2′-bpy planes about 3.471 Å (Supporting Information Figure S2b). The adjacent dimeric chains are further aggregated together to yield a 2D supramolecular layer via countercation $\{Cu((2,2'\text{-bpy})_2\}$ with supramolecular interaction (N4···O4 3.039 Å, Supporting Information Figure S2c). The 3D supramolecular framework was generated (Supporting Information Figure S2d) by supramolecular interaction between different 2D layers with weak interaction (C1··· O13 3.408 Å and C1···O5 3.205 Å).

Structure of $[H_2(4,4'\text{-bpy})]_{2.5}[As^{III}(As_2{}^{V}Mo_2{}^{V}Mo_{16}{}^{VI}O_{62})]\cdot 5H_2O$ (2). Compound **2** is built up of one asymmetric monocapped Dawson polyoxoanion $\{As^{III}(As_2{}^{V}Mo_2{}^{V}Mo_{16}{}^{VI}O_{62})\}^{5-}$ cluster, two and a half biprotonated 4,4′-bipy ligands, and five lattice water molecules (Supporting Information Figure S3). The anion can be described as a classic Well−Dawson cluster $\{As_2Mo_{18}\}$ capped by one As^{III} atoms on one pit position of $\{Mo_3O_{13}\}$ trimer located in one "polar" position of the Dawson framework (Figure 2). The

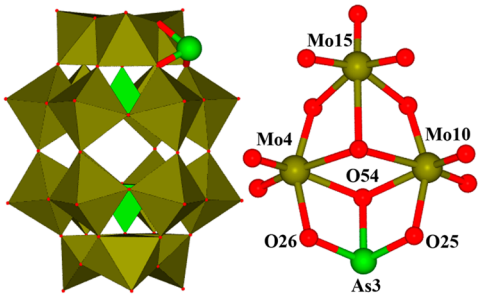

Figure 2. Monoarsenate capped Dawson arsenomolybdate and the coordination environment of As atom in **2**.

pyramidal-linked $\{AsO_3\}$ caps on pit positions of $\{Mo_3O_{13}\}$ are formed through the ligation of three μ-O atoms to one As atom. The As−O distances range from 1.806(14) to 1.875(15) Å. The O−As−O bond angles are in the range of 82.1(6)−103.0(6)°. It is noteworthy that two monocapped polyoxoanions are linked by supramolecular interactions between As(III)-cap and μ-O atoms of two adjacent Dawson anions (As3···O54 3.081 Å) to form a dimeric cluster (see Supporting Information Figure S4a). The adjacent dimeric clusters are stably packed together by surface oxygen atoms of a Dawson cluster and exhibit 1D supramolecular chain with supramolecular interactions (O22···O59 2.988 Å). The lattice water molecules link the 1D chains into the 2D supramolecular layer (Supporting Information Figure S4b) through a pair of hydrogen bonds O1W···O33:3.17(3) Å and O1W··· O37:3.07(3) Å (shown in Supporting Information Table S2). Moreover, these adjacent 2D layers are further linked together by protonated 4,4′-bipy to lead to an extending 3D structure (Supporting Information Figure S4c). The typical supramolecular interactions are N4−O16 2.918, N5−O32 2.970, and N5−C22 2.767 Å. All protonated 4,4′-bipy units and solvent water molecules reside in the interspaces between two adjacent supramolecular layers.

Structure of $(pyr)(imi)(Himi)_3[As_2{}^{III}(As_2{}^{V}Mo_3{}^{V}Mo_{15}{}^{VI}O_{62})]\cdot 3H_2O$ (3). The basic units of compound **3** consist of one symmetric bicapped Dawson $\{As_2{}^{III}(As_2{}^{V}Mo_3{}^{V}Mo_{15}{}^{VI}O_{62})\}$anion cluster, one Pyr and imi, three Himi organic ligands, and three lattice water molecules (Supporting Information Figure S5). It is remarkable in structure **3** that four $\{As^{III}\}$ subunits cap onto four symmetric pit positions of the $\{Mo_3O_{13}\}$ trimer located two "polar" positions of the Dawson framework (Figure 3). The same pyramidal-linked

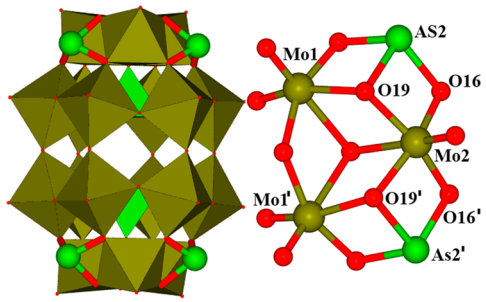

Figure 3. Biarsenate capped Dawson arsenomolybdate and the coordination environment of As atom in **3**.

$\{AsO_3\}$ caps on the $\{Mo_3O_{13}\}$ pit are formed through the combination of three μ-O atoms to one As atom. Different from that in **2**, the occupation ratio of As at the As(2) position is 0.5, which is the only reported example with this kind of connection mode for a bicapped Dawson cluster. The As−O average distance is 1.895 Å. The O−As−O bond angles are in the range 84.3(4)−107.2(4)°. In compound **3**, owing to half occupation of As2, the structure of bicapped Dawson is discrete clusters. There are three kinds of positional isomers for disordered positions of the As(III) capping groups (Supporting Information Figure S6). Compound **3** can be viewed as the product of the coexistence of three isomers. The adjacent bicapped Dawson clusters are aggregated together via hydrogen bond interactions (O2W···O6 2.95(6) Å) between O atoms of lattice water molecules and terminal O atoms of Dawson clusters to form 1D chains (Supporting Information Figure S7a). The chain is further arranged through means of supramolecular interaction (As2···O16 3.192 Å) giving birth to an infinite 2D supramolecular layer (Supporting Information Figure S7b). The isolated water and imi molecules link the 2D supramolecular layers into an extending 3D network (Supporting Information Figure S7c) through hydrogen bonds (O1W··· O18 2.956 Å) and supramolecular interactions (C4···O17 3.021 and O1W···C6 2.816 Å).

Structure of $[As_3{}^{III}(As_2{}^{V}Mo_3{}^{V}Mo_{15}{}^{VI}O_{62})]\cdot 4H_2O$ (4). Compound **4** is composed of another kind of tricapped Dawson $\{As_3{}^{III}(As_2{}^{V}Mo_3{}^{V}Mo_{15}{}^{VI}O_{62})\}$ cluster and four water molecules (Supporting Information Figure S8). Different from compound **3**, compound **4** is a tricapped cluster (Figure 4), which can be described as Dawson cage $\{As_2Mo_{18}\}$ capped by six $\{As^{III}\}$ atoms on six symmetric pit positions of the $\{Mo_3O_{13}\}$ trimer located at two "polar" positions of the Dawson cluster. The pyramidal-linked $\{AsO_3\}$ caps on the $\{Mo_3O_{13}\}$ pit are formed through the linkage of three μ-O atoms to one As atom. It is worth noting that the occupation ratio of all As atoms at the

dx.doi.org/10.1021/ic5014973 | Inorg. Chem. 2014, 53, 12337−12347

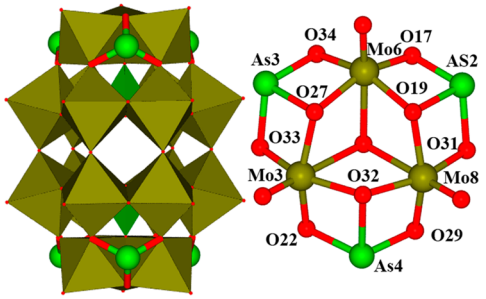

Figure 4. Triarsenate capped Dawson arsenomolybdate and the coordination environment of As atom in **4**.

As(2), As(3), and As(4) positions are 0.5. The As−O average distance is 1.975 Å. The O−As−O bond angles are in the range 85.4(8)−106.9(9)°. It is more meaningful that all the ditches of the $\{Mo_3O_{13}\}$ unit are filled in the form of arsenic cap via adjusting the pH value from 3 to 2. For compound **4**, Dawson clusters also should be 0D clusters due to half occupation of As. There are 10 kinds of positional isomers for disordered positions of the As(III) capping groups (Supporting Information Figure S9). Compound **4** can be viewed as the product of the coexistence of these isomers. Each neutral tricapped cluster is connected to four coplanar Dawson clusters via two pairs of supermolecular interactions (O18···O30 3.006 Å and O24···O20 3.007 Å) to form the 2D layer (Supporting Information Figure S10a). Supermolecular and hydrogen bond interactions between oxygen atoms of water molecules and terminal oxygen atoms of Dawson cluster are also found to stabilize the 3D supramolecular framework (Supporting Information Figure S10b). The typical weak interactions are O25···O3W 3.006 Å and O3W···O26 2.973 Å.

Structures of $(H_2btp)_3[As_2{}^{V}Mo_{18}{}^{VI}O_{62}]\cdot 6H_2O$, (5). Compound **5** is composed of a Dawson $\{As_2Mo_{18}{}^{VI}O_{62}\}$ cluster, three protonated H_2btp organic ligands, and four lattice water molecules (Supporting Information Figure S11). Two protonated H_2btp ligands are bonded to two terminal oxygen atoms of the $\{As_2Mo_{18}\}$ anion to form a bisupported structure (Figure 5a) via supramolecular interaction (N17···O20 3.028 Å and N7···O54 2.997 Å). The adjacent bisupported polyoxoanion clusters are aggregated together via supramolecular interactions (O38···O54 3.032 Å) to form an infinite 1D chain (Figure 5b). The isolated water molecules link the chains into the 2D supramolecular layer (Figure 5c) through a pair of hydrogen bonds (O3W···O9 2.811(5) Å and O3W···O29 2.857 Å). The adjacent 2D layers are further aggregated together to yield a 3D supramolecular network in ABAB mode via lattice water molecules with supramolecular interaction (O58···O6W 2.923 Å and O6W···O59 2.901 Å, Figure 5d). Furthermore, weak hydrogen bonding interactions (C−H···O) exist between organic ligands and the Dawson cluster to stabilize the whole supramolecular structure. Therefore, protonated organic ligands play important roles in inducing the supramolecular framework during the self-assembly process. They play dual roles: charge-balance and structure direction via hydrogen bands or supramolecular interactions.

IR Spectroscopy. The IR spectra of compounds **1**−**5** recorded between 400 and 4000 cm^{-1} with KBr pellet (see Supporting Information, Figure S12a−e) are similar: the peaks at 992−985 cm^{-1} are attributed to ν(As—O_a) vibrations; the strong peaks at 904−875 cm^{-1} are ascribed to ν(Mo═O_t) vibrations; peaks at 834−764 cm^{-1} are assigned to ν(Mo—O_b) vibrations; the peaks locate at 756−665 cm^{-1} can be attributed to ν(Mo—O_c).[21a] The strong peaks at 1508−1416 cm^{-1} are indicative of ν(C—N) vibrations of organic ligands. Furthermore, the broad peaks between 3250 and 3432 cm^{-1} and the peaks at 1654−1623 cm^{-1} can be assigned to ν(N—H) and/or ν(O—H) of the protonated organic ligands and water molecules.

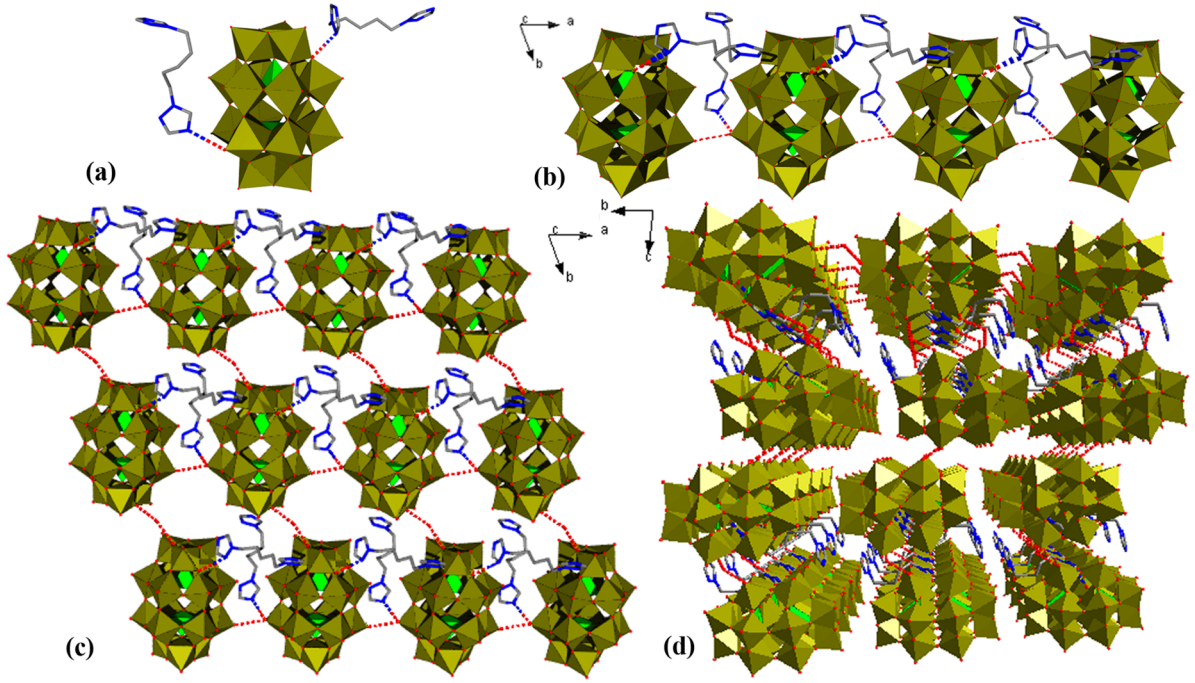

Figure 5. (a) Basic building unit of compound **5**; (b) 1D straight chain of compound **5** based on $\{As_2Mo_{18}\}$ units and pyz ligands via hydrogen bond interactions; (c) 2D supramolecular layer in compound **5**; (d) 3D supramolecular network in ABAB mode in the *ac* plane of compound **5**.

dx.doi.org/10.1021/ic5014973 | *Inorg. Chem.* 2014, 53, 12337−12347

UV−Vis−NIR Spectroscopy. The UV−vis−NIR absorption spectra of compounds **1**−**5** are presented in Supporting Information Figure S13a−e. The two strong bands in the ranges 210−235 and 285−310 nm are attributed to (LMCT) $p\pi$(Oterminal) → $d\pi^*$(Mo) electronic transitions in the Mo═O bonds and $d\pi-p\pi-d\pi$ electronic transitions between the energetic levels of the Mo—O—Mo bonds, respectively.[21b] The broad band at 580−620 and 1100−1180 nm for compounds **1**−**4** ascribed to overlap of two bands of the intervalence transition from the Mo^{V} to Mo^{VI} via the Mo—O—Mo bond and the d−d transitions of Mo^{V} octahedral,[21] leading to the dark blue color of compounds **1**−**4**. In addition, the Cu—$N_{(bpy)}$ and Cu—$O_{(POM)}$ LMCT bands are also ascribed to the broad band for **1**.[22]

XPS Spectroscopy. The oxidation states of As, Mo, Cu are further confirmed by X-ray photoelectron spectroscopy (XPS) measurements, which were carried out in the energy region of As $3d_{5/2}$ and As $3d_{3/2}$, Mo$3d_{5/2}$ and Mo$3d_{3/2}$, Cu $2p_{1/2}$ and Cu $2p_{3/2}$, respectively (Supporting Information Figure S14a−e). The XPS spectrum of compounds **1**−**4** presents four overlapped peaks at 230.8−231.2, 232.3−232.5, 235.3−235.5, and 234.1−234.4 eV in the Mo 3d region, which should be ascribed to the mixture of Mo^{5+} and Mo^{6+}, respectively.[23a] The XPS results also support the BVS calculations for the Mo oxidation states, in which the deconvolution of the spectra indicates that the ratio of Mo^{VI}/Mo^{V} is about 8:1 for compounds **1** and **2**, and about 5:1 for compounds **3** and **4**, respectively. The peaks at 232.3 and 235.5 eV in the Mo 3d region for **5** are attributed to Mo^{6+} ($3d_{5/2}$) and Mo^{6+} ($3d_{3/2}$), respectively. The four peaks at 39.0−39.3, 40.2−40.4, 43.2−43.5, and 44.9−45.0 eV in the As3d region for **2**−**4** are assigned to As^{3+} ($3d_{5/2}$), As^{5+} ($3d_{5/2}$), As^{3+} ($3d_{3/2}$), and As^{5+} ($3d_{3/2}$), respectively. Two peaks at 39.9 and 44.7 eV for **1**, and 39.8 and 44.5 eV for **5**, are ascribed to As^{5+} ($3d_{5/2}$) and As^{5+} ($3d_{3/2}$), respectively.[8] The peaks at 932.4 and 954.1 eV for **1** are ascribed to Cu^{2+} ions.[8b] These XPS estimations obtained on the valence state values seem to be reasonably consistent with those calculated from the bond valence sum calculations. These results are also in good agreement with the structure analyses.

TG Analyses. The thermal stabilities of compounds **1**−**5** were investigated under a N_2 atmosphere from 40 to 600 °C, and the TG curves are showed in Supporting Information Figure S15a−e. In the TG curve of compound **1**, the first weight loss of 1.61% (calcd 1.81%) at 100−205 °C corresponds to the loss of four lattice water molecules. The second weight loss between 230 and 375 °C of 21.14% arises from the loss of all 2,2′-bpy molecules (calcd 19.64%, for 5 bpy). For **2**, the first weight loss of 2.08% (calcd 2.63%) at 163−182 °C is attributed to five lattice water molecules. The second and third weight losses of 17.50% at 285−435 °C are assigned to the removal of two and a half 4,4′-bpy ligands and one As_2O_3 escaping (calcd 17.27%). For **3**, the first weight loss of 2.02% in the temperature 120−185 °C is due to the loss of all lattice water molecules (calculated value 1.58% for $3H_2O$). The second weight loss of 9.82% between 200−320 °C arises from the loss of all of imi and pyr organic ligands (calcd 10.19%, for 1 py, 1 imi, and 3 Himi). The third weight loss of 11.08% between 325 and 450 °C is assigned to the removal of most of the As_2O_3 escaping. The value is close to the calculated value of 11.57% (for $2As_2O_3$). For **4**, the first weight loss of 2.48% at 140−180 °C corresponds to the loss of discrete water molecules (calcd 2.26%, for $4H_2O$). The second weight loss between 345 and 425 °C of 18.46% relates from the evacuation of all As_2O_3 molecules (calcd 18.64%, for $3As_2O_3$). The TG curves of compound **5** exhibit two step weight loss: the first weight losses of 2.82% (calcd 3.01%) at 148−220 °C correspond to the loss of six lattice water molecules. The second weight losses between 234 and 325 °C of 17.66% arise from the loss of all the btp molecules (calcd 17.21%, for 3 btp). All the weight losses from the TG curves are in accord with the formulas of compounds **1**−**5**.

XRPD Analysis. The simulated and experimental the X-ray power diffraction (XRPD) patterns of the title compounds are presented in Supporting Information Figure S16. The diffraction peaks of both simulated and experimental patterns match in the key positions, indicating the phase purity of the compounds. The difference in intensity may be due to the preferred orientation of the powder samples.

EPR Spectroscopy. The ESR spectra for compounds **1**−**4** were measured in the solid state at low temperature (77 K). The ESR spectrum of compound **1** shows one approximate axially symmetric ESR signal with $g_{\|}$ = 2.348, $g_{\perp}$ = 2.083, $A_{\|}$ = 10.2 mT, and $A_{\perp}$ = 1.53 mT (Supporting Information Figure S17a). The larger A value (10.2 mT) in the parallel component of the axially symmetrical ESR signal was suggested to reflect a square pyramidal Cu ion environment. Such spectra agree with the compound consisting of octahedral and square pyramidal Cu ion coexistence, which is consistent with literature data.[23b] The ESR spectra of **1** show no signals for Mo^{V}. The absence of ESR signals indicates that the electrons of the Mo^{V} are antiferromagnetically coupled at low temperature. The EPR spectra of **2**−**4** show that the single unpaired electrons are trapped attributing to Mo^{V} with g = 1.932 for **2**, $g_{1,2,3}$ = 1.882, 1.924, and 1.953 for **3**, and $g_{1,2,3}$ = 1.863, 1.918, and 1.949 for **4** (shown in Supporting Information Figure S17b−d). It is noteworthy that the anisotropic hyperfine structures are observed in EPR spectra of **3** and **4**, which show that different "blue" electron numbers will lead to different structure distortion degree.

Electrochemical and Electrocatalytic Properties. Although compounds **1**−**5** were obtained from the aqueous system, they cannot be dissolved in water or acidic aqueous solution; therefore, their electrochemical behavior was investigated with **1**−**5**-modified carbon paste electrodes (**1**−**5**-**CPE**). The cyclic voltammetric behaviors of **1**−**5**-**CPE** in 1 M H_2SO_4 aqueous solution at different scan rates were recorded in the potential range from 1.0 to −1.0 V (see Supporting Information Figure S18a−e). The CVs of **1**−**5**-**CPE** show reversible redox peaks with the half-wave potentials $E_{1/2} = (E_{pa} + E_{pc})/2$ at +0.07, and −0.25 V for **1**, +0.46, +0.06, and −0.29 V for **2**, +0.42, +0.01, and −0.28 V for **3**, +0.55, +0.14, and −0.21 V for **4**, 0.43, −0.012, and −0.33 V for **5**, respectively (based on the CV at 20 mV s^{-1}, Supporting Information Figure S19a−e), ascribed to consecutive two-electron processes of a Dawson-type arsenomolybdate framework.[24] Although compounds **1**−**5** contain similar parent cluster units, the mean peak potentials are slightly different, due to their different capping environments and the number of "blue" electrons. The cathodic peak potentials of all compounds **1**−**5** shift toward the negative direction, and the corresponding anodic peak potentials shift to the positive direction with increasing scan rates, as shown in Supporting Information Figure S18. The peak potentials change gradually following the scan rate from 20 to 500 mV s^{-1}. Moreover, the peak-to-peak separations between the corresponding anodic and cathodic peaks increased, but the average peak potentials do not change on the whole. The plots

dx.doi.org/10.1021/ic5014973 | Inorg. Chem. 2014, 53, 12337−12347

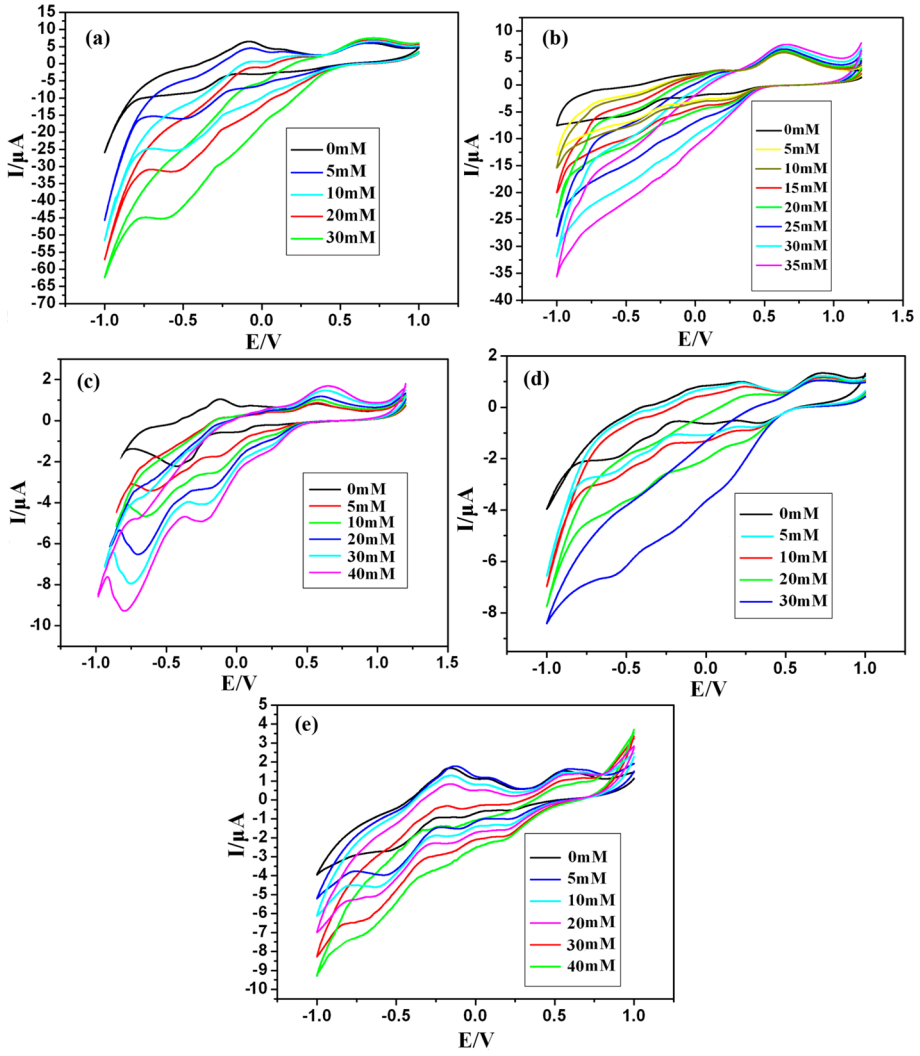

Figure 6. Cyclic voltammograms of (a) **1**-, (b) **2**-, (c) **3**-, (d) **4**-, and (e) **5-CPE** in 1 M H_2SO_4 solution containing nitrite at different concentrations (potentials vs SCE; scan rate 20 mV s^{-1}).

of anodic and cathodic peak current (II) versus scan rates (see insert plots in Supporting Information Figure S18) indicate that the redox processes of **1**−**5-CPE** are surface-controlled below the scan rate of 100 mV s^{-1}, while at scan rates higher than 100 mV s^{-1}, the peak currents were proportional to the square root of the scan rate, suggesting that redox processes are diffusion-controlled.[25] It is also noteworthy that **1**−**5-CPE** possesses the high stability. When the potential range is maintained between −0.1 and 1.0 V, the peak currents remain almost unchanged over 300 cycles at a scan rate 100 mV s^{-1}.

Furthermore, **1**−**5-CPE** displays good electrocatalytic activity on reduction of nitrite (Figure 6). At **1**−**5-CPE**, with the addition of $NaNO_2$, all reduction peak currents increased while the corresponding oxidation peak currents dramatically decreased, suggesting that $NaNO_2$ was reduced by all five polyoxoanion species.[25a] It has been noted that the shift of the uncapped kind (compound **1**) is relatively weaker than those of the copper(II) and arsenate(III) capped kind, which proved that the catalytic activities were enhanced with the increasing extent of cap for the parent cluster unit.

The electrocatalytic efficiency (CAT) of **1**-CPEs can be calculated by using the CAT formula[25b]

$$\mathrm{CAT} = 100\% \times [I_p(\mathrm{POM, substrate}) - I_p(\mathrm{POM})] / I_p(\mathrm{POM})$$

where I_p(POM, substrate) and I_p(POM) are the peak currents for the reduction of the POM with and without the presence of substrate (NO_2^-), respectively. Compared with **2**−**4**-CPE, the **1**-CPE shows a high CAT value (419%) toward 30 mM NO_2^- (Figure 7), which may be due to the introduction of the {Cu(bipy)} complex cap. The bipy with rich π-electron may favor electron exchanges during the electrocatalytic process, which is a possible main reason why **1**−CPE possesses good electrocatalytic avtivity. In addition, **2**-, **3**-, and **4**-CPE show a higher CAT value toward 30 mM NO_2^- (224%, 258%, and 240%, respectively) than **5**-CPE (134%), which may be owing to the synergetic effect of Mo and As^{III} ions in capped Dawson clusters.

Fluorescent Properties. The solid-state emission spectra of compounds **1**, **2**, **3**, and **5** at room temperature are depicted in Supporting Information Figure S20. Compound **1** exhibits intense emission maxima at ca. 462 nm (Supporting Information Figure S20a, λ_{ex} = 380). According to the literature,[26] the emission can be assigned to the emission of ligand-to-metal charge transfer (LMCT). It is known that the

dx.doi.org/10.1021/ic5014973 | Inorg. Chem. 2014, 53, 12337−12347

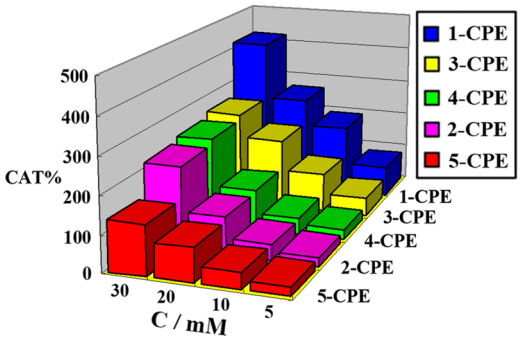

Figure 7. Chart of the CAT vs concentration of NO_2^- for **1**−**5**-CPE. I_p values of cathodic peak I for NO_2^- at a scan rate 50 mV s^{-1}.

free 2,2′-bpy molecule displays a weak luminescence at ca. 530 nm in the solid state at room temperature. The blue shifts and the luminescent enhancement compared to those of a free 2,2′-bpy molecule may be due to the chelation of the 2,2′-bpy ligand to the metal ion, which effetively increases the rigidity of the ligand and reduces the loss of energy by radiationless decay of the intraligand emission excited state.[27] The emission spectra of compounds **2** and **5** are also observed as intense emissions occurring at 435 and 438 nm, respectively (Supporting Information Figure S20b and λ_{ex} = 375 and 360 nm, respectively). According to previous observations,[28] these peaks are close to the emission band of free 4,4′-bpy (437 nm) and btp (450 nm) ligands attributed to the intraligand emission from the protonated 4,4′-bpy and btp emission ligand, respectively.[29] The maximum emission band occurs at 425 nm upon excitation at 348 nm for **3** (Supporting Information Figure S20c). The peak at 425 nm is different from that of free pyrazine (449 nm) or imidazole (389 nm) ligand, which is attributed to the intraligand emission between the protonated pyr and imi ligand or ligand-to-POM charge transfer.[30] These observations indicate that the photoluminescence properties of POMs could be adjusted by changing their structures and compositions. The compounds may be excellent candidates for potential solid-state photofunctional materials, since they are thermally stable and insoluble in common polar and nonpolar solvents.

Magnetic Properties. The variable temperature magnetic susceptibilities of **1** were measured from 300 to 2 K at 1000 Oe and plotted as $\chi_m T$ and χ_m versus T, as shown in Figure 8a. The $\chi_m T$ product of 1.62 cm^3 K mol^{-1} at 300 K decreases continuously to 1.21 cm^3 K mol^{-1} at 1.8 K. The $\chi_m T$ value at room temperature is much lower than the spin-only value (g = 2.0) of 2.25 cm^3 K mol^{-1} for four Cu^{2+} and two Mo^V noninteracting ions ($S = {}^1/_2$), but close to the value of 1.51 cm^3 K mol^{-1} (μ_{eff} = 3.46 μ_B determined from equation $\mu_{eff} = 2.828(\chi_m T)^{1/2}$) for four isolated Cu^{2+} ions. This result suggests that all delocalized electrons in the polyoxoanion cluster might be totally antiferromagnetically coupled, which had been observed in previous literature.[31] The $1/\chi_m$ versus T curve is consistent with the Curie−Weiss law with C = 1.63 cm^3 K mol^{-1} and θ = −6.52 K, indicating the presence of weak antiferromagnetic behavior in the whole compound (Supporting Information Figure S21). In compound **2** (shown in Figure 8b), the largest effective magnetic moment μ_{eff} is 2.47 μ_B ($\chi_m T$ = 0.76 cm^3 K mol^{-1}) at 18 K, close to the expected spin-only value for two Mo^V (2.45 μ_B). The increase in the magnetic moment with decreasing temperature indicates ferromagnetic exchange interactions among two Mo^V ions. However, the $\chi_m T$ product of **2** decreased rapidly at very low temperatures, which might be mainly attributed to the presence of zero-field splitting. The behavior suggests that there exist overall ferromagnetic interactions with the presence of zero-field splitting for two Mo^V ions in compound **2**. The magnetic properties of **3** and **4** are shown in Figure 8c,d. The effective magnetic moment of 1.76 and 1.74 μ_B per cluster anion at room

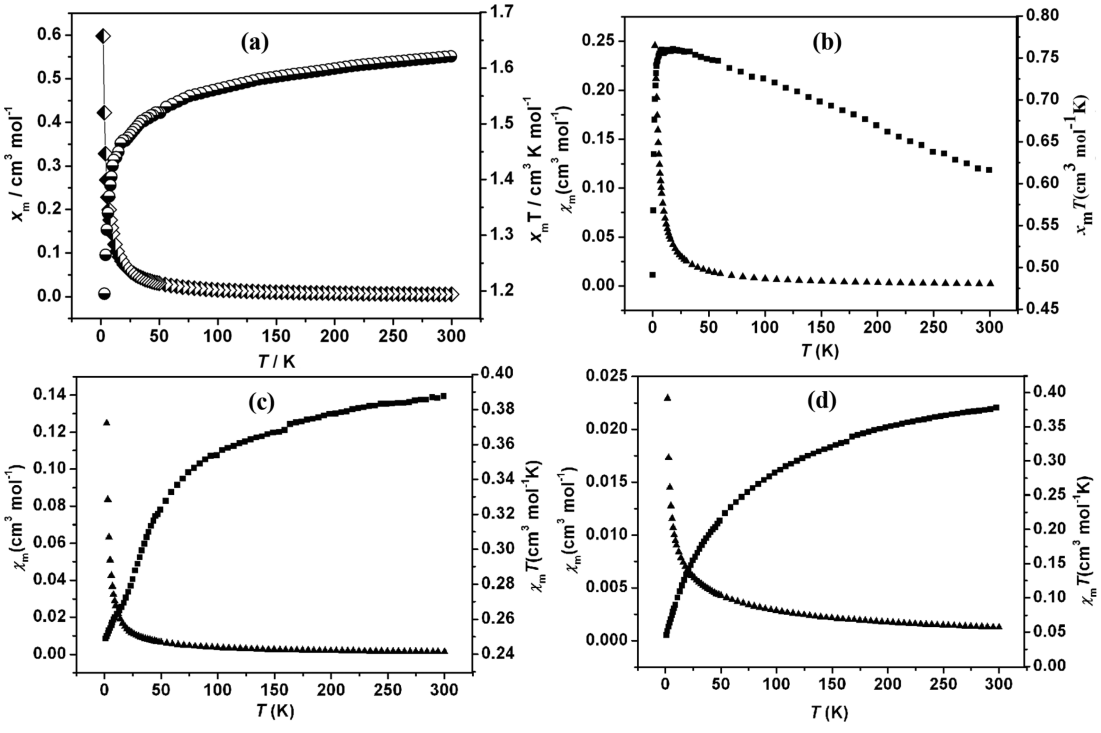

Figure 8. Plot of χ_m and $\chi_m T$ versus T for (a) compound **1**, (b) compound **2**, (c) compound **3**, and (d) compound **4**.

dx.doi.org/10.1021/ic5014973 | Inorg. Chem. 2014, 53, 12337−12347

temperature, which is slightly higher than the spin-only value of 1.73 μ_B, may partly be due to a positive, temperature-independent contribution from the coupling of ground and excited state levels through Zeeman perturbation, and to orbital contributions of the Mo^V d^1 ion. The temperature-dependent magnetic measurements suggest that only one electron is unpaired the other two "blue" electrons are antiferromagnetically coupled. Similar behavior in a heteropolyanion has been observed before.[32]

CONCLUSION

In this Article, certain numbers of Cu^{2+} or As^{3+} are introduced into a Well−Dawson $\{As_2Mo_{18}\}$ system to act as cap, which leads to five novel arsenomolybdates. Our result further suggests that the kind, number, and location of cap may be controlled by altering pH and organic ligand of the reaction system. **1**−**5-CPE** display unique redox properties and good electrocatalytic activity to reduce nitrite. The studies of CAT indicate that introduction of cap units can enhance the catalytic activity of the Dawson cluster. Fluorescent analysis exhibits that compounds **1**, **2**, **3**, and **5** are potential fluorescence-emitting materials. Furthermore, compounds **1**−**4** reveal different magnetic interactions between the metal centers for their different structures. This work enriches Wells−Dawson-based inorganic−organic hybrid materials and provides a useful prototype for design and synthesis of capped Dawson hybrids.

ASSOCIATED CONTENT

Supporting Information

X-ray crystallographic files for compounds **1**−**5** in CIF format and tables of selected bond lengths (Å) and bond angles (deg) for compounds **1**−**5**; plots of IR, XPS, XRD, and UV−vis−NIR spectra; TG curves; voltammetric behaviors; fluorescence spectra for **1**−**5**; and partial structural figures of compounds **1**−**5**. This material is available free of charge via the Internet at http://pubs.acs.org.

AUTHOR INFORMATION

Corresponding Authors

*E-mail: hlyukai@163.com.

*E-mail: zhou_bai_bin@163.com.

Notes

The authors declare no competing financial interest.

ACKNOWLEDGMENTS

This work was supported by the National Natural Science Foundation of China (Grants 21271056 and 21371042), the Ministry of Education and Specialised Research Fund for the Doctoral Program of Higher Education (20122329110001), the Natural Science Foundation of Heilongjiang Province (B201216), Key Laboratory of Functional Inorganic Material Chemistry (Heilongjiang University), Ministry of Education, Doctoral Initiation Foundation of Harbin Normal University (No. KGB201214), and Program for Scientific and Technological Innovation Team Construction in Universities of Heilongjiang Province (No. 2011TD010).

REFERENCES

(1) (a) Gouzerh, P.; Proust, A. *Chem. Rev.* **1998**, *98*, 77. (b) Sun, M.; Zhang, J. Z.; Putaj, P.; Caps, V.; Lefebvre, F.; Pelletier, J.; Basset, J. M. *Chem. Rev.* **2014**, *114*, 981. (c) Sumliner, J. M.; Lv, H. J.; Fielden, J.; Geletii, Y. V.; Hill, C. L. *Eur. J. Inorg. Chem.* **2014**, 635.

(2) (a) Li, J. R.; Tao, Y.; Yu, Q.; Bu, X. H.; Sakamoto, H.; Kitagawa, S. *Chem.—Eur. J.* **2008**, *14*, 2771. (b) Getman, R. B.; Bae, Y. S.; Wilmer, C. E.; Snurr, R. Q. *Chem. Rev.* **2012**, *112*, 703. (c) Liu, D.; Lu, Y.; Tan, H. Q.; Chen, W. L.; Zhang, Z. M.; Li, Y. G.; Wang, E. B. *Chem. Commun.* **2013**, *49*, 3673.

(3) (a) Long, D. L.; Burkholder, E.; Cronin, L. *Chem. Soc. Rev.* **2007**, *36*, 105. (b) Zeng, Y. F.; Hu, X.; Liu, F. C.; Bu, X. H. *Chem. Soc. Rev.* **2009**, *38*, 469. (c) Lydon, C.; Busche, C.; Miras, H. N.; Delf, A.; Long, D. L.; Yellowlees, L.; Cronin, L. *Angew. Chem., Int. Ed.* **2012**, *51*, 2115. (d) Liu, X. C.; Xing, Y.; Wang, X. L.; Xu, H. B.; Liu, X. Z.; Shao, K.; Su, Z. M. *Chem. Commun.* **2010**, *46*, 2614.

(4) (a) Horcajada, P.; Gref, R.; Baati, T.; Allan, P. K.; Maurin, G.; Couvreur, P.; Férey, G.; Morris, R. E.; Serre, C. *Chem. Rev.* **2012**, *112*, 1232. (b) Wang, L.; Zhou, B. B.; Yu, K.; Su, Z. H.; Gao, S.; Chu, L. L.; Liu, J. R.; Yang, G. Y. *Inorg. Chem.* **2013**, *52*, 5119.

(5) (a) Yin, P.; Pradeep, C. P.; Zhang, B. F.; Li, F. Y.; Lydon, C.; Rosnes, M. H.; Li, D.; Bitterlich, E.; Xu, L.; Cronin, L.; Liu, T. B. *Chem.—Eur. J.* **2012**, *18*, 8157. (b) Du, M.; Guo, Y. M.; Chen, S. T.; Bu, X. H.; Batten, S. R.; Ribas, J.; Kitagawa, S. *Inorg. Chem.* **2004**, *43*, 1287. (c) Omwoma, S.; Chen, W.; Tsunashima, R.; Song, Y. F. *Coord. Chem. Rev.* **2014**, *58*, 258. (d) Marcì, G.; García-López, E. I.; Palmisano, L. *Eur. J. Inorg. Chem.* **2014**, 21.

(6) (a) Lü, J.; Lin, J. X.; Zhao, X. L.; Cao, R. *Chem. Commun.* **2012**, *48*, 669. (b) Sha, J. Q.; Liang, L. Y.; Sun, J. W.; Tian, A. X.; Yan, P. F.; Li, G. M.; Wang, C. *Cryst. Growth Des.* **2012**, *12*, 894. (c) Walsh, J. J.; Mallon, C. T.; Bond, A. M.; Keyes, T. E.; Forster, R. J. *Chem. Commun.* **2012**, *48*, 3593. (d) Wang, X.; Peng, J.; Liu, M. G.; Wang, D. D.; Meng, C. L.; Li, Y.; Shi, Z. Y. *CrystEngComm* **2012**, *14*, 3220. (e) Han, Q. X.; Sun, X. P.; Li, J.; Ma, P. T.; Niu, J. Y. *Inorg. Chem.* **2014**, *53*, 2006.

(7) (a) Yang, Y. Y.; Xu, L.; Jia, L. P.; Gao, G. G.; Li, F. Y.; Qu, X. S.; Qiu, Y. F. *Cryst. Res. Technol.* **2007**, *10*, 42. (b) Yu, H. H.; Zhang, X.; Kong, L.; Xu, J. Q. *Acta Crystallogr.* **2009**, 1698. (c) Soumahoro, T.; Burkholder, E.; Ouellette, W.; Zubieta, J. *Inorg. Chim. Acta* **2005**, *358*, 606. (d) Zhang, X. T.; Wei, P. H.; Shi, C. W.; Lia, B.; Hu, B. *Acta Crystallogr.* **2010**, *E66*, 174.

(8) (a) Han, Q. X.; Ma, P. T.; Zhao, J. W.; Wang, Z. L.; Yang, W. H.; Guo, P. H.; Wang, J. P.; Niu, J. Y. *Cryst. Growth Des.* **2011**, *11*, 436. (b) Niu, J. Y.; Hua, J. I.; Ma, X.; Wang, J. P. *CrystEngComm* **2012**, *14*, 4060.

(9) (a) Hou, D.; Hagen, K. S.; Hill, C. L. *J. Chem. Soc., Chem. Commun.* **1993**, 426. (b) Chen, Q.; Hill, C. L. *Inorg. Chem.* **1996**, *35*, 2403. (c) Dolbecq, A.; Cadot, E.; Eisner, D.; Sécheresse, F. *Inorg. Chem.* **1999**, *38*, 4217. (d) Zhang, Y.; Haushalter, R. C.; Clearfield, A. *J. Chem. Soc., Chem. Commun.* **1995**, 1149. (e) Liu, J.; Xu, J. N.; Liu, Y. B.; Lu, Y. K.; Song, J. F.; Zhang, X.; Cui, X. B.; Xu, J. Q.; Wang, T. G. *J. Solid. State. Chem.* **2007**, *180*, 3456. (f) Yang, W. B.; Lu, C. Z.; Zhan, X. P.; Zhuang, H. H. *Inorg. Chem.* **2002**, *41*, 4621.

(10) (a) Compain, J. D.; Nakabayashi, K.; Ohkoshi, S. I. *Polyhedron* **2013**, *66*, 116. (b) Barats-Damatov, D.; Shimon, L. J. W.; Neumann, R. *Eur. J. Inorg. Chem.* **2013**, 1649.

(11) Li, X. X.; Zheng, S. T.; Fang, W. H.; Yang, G. Y. *Inorg. Chem. Commun.* **2011**, *14*, 1541.

(12) Feng, M. L.; Mao, J. G. *Eur. J. Inorg. Chem.* **2004**, 3712.

(13) (a) Huang, J.; Han, Z. G.; Zhang, H.; Yu, H. T.; Zhai, X. L. *J. Solid. State. Chem.* **2012**, *194*, 65. (b) Shi, S. Y.; Teng, H. H.; Chang, L. M.; Wang, Y.; Xiao, L. N.; Cui, X. B.; Xu, J. Q. *Inorg. Chim. Acta* **2013**, *399*, 172.

(14) Cao, Y. N.; Zhang, H. H.; Huanga, C. C.; Yang, Q. Y.; Chen, Y. P.; Sun, R. Q.; Zhang, F. L.; Guo, W. J. *J. Solid. State Chem.* **2005**, *178*, 3563.

(15) (a) Burholder, E.; Golub, V.; O'Connor, C. J.; Zubieta, J. *Chem. Commun.* **2003**, 2128. (b) Fu, R. B.; Wu, X. T.; Hu, S. M.; Zhang, J. J.; Fu, Z. Y.; Du, W. X.; Xia, S. Q. *Eur. J. Inorg. Chem.* **2003**, 1798. (c) Kortz, U.; Marquer, C.; Thouvenot, R.; Nierlich, M. *Inorg. Chem.* **2003**, *42*, 1158. (d) Burholder, E.; Golub, V.; O'Connor, C. J.; Zubieta, J. *Inorg. Commun.* **2003**, *42*, 6729. (e) Kortz, U. *Inorg. Chem.* **2000**, *39*, 625.

(16) Kortz, U.; Savelieff, M. G.; Ghali, F. Y. A.; Khalil, L. M.; Maalouf, S. M.; Sinno, D. I. *Angew. Chem., Int. Ed.* **2002**, *41*, 4070.
(17) Sun, C. Y.; Li, Y. G.; Wang, E. B.; Xiao, D. R.; An, H. Y.; Xu, L. *Inorg. Chem.* **2007**, *46*, 1563.
(18) (a) Sheldrick, G. M. *SHELXL 97, Program for Crystal Structure Refinement*; University of Göttingen: Göttingen, Germany, 1997. (b) Sheldrick, G. M. *SHELXL 97, Program for Crystal Structure Solution*; University of Göttingen: Göttingen, Germany, 1997.
(19) (a) Zhao, Z. F.; Zhou, B. B.; Su, Z. H.; Ma, H. Y.; Li, C. X. *Inorg. Chem. Commun.* **2008**, *11*, 648. (b) Su, F. Y.; Zhou, B. B.; Zhao, Z. F.; Su, Z. H.; Zhu, C. C. *Cryst. Res. Technol.* **2009**, *44*, 447.
(20) (a) Brown, I. D.; Altermatt, D. *Acta. Crystallogr., Sect. B* **1985**, *41*, 244. (b) Liu, W.; Thorp, H. H. *Inorg. Chem.* **1993**, *32*, 4102.
(21) (a) Yang, Y. Y.; Xu, L.; Jia, L. P.; Gao, G. G.; Li, F. Y.; Qu, X. S.; Qiu, Y. F. *Cryst. Res. Technol.* **2007**, *42*, 1036. (b) Pope, M. T. *Heteropoly and Isopoly Oxometalates*; Springer-Verlag: Berlin, 1983.
(22) DasGupta, B.; Katz, C.; Israel, T.; Watson, M.; Zompa, L. *Inorg. Chim. Acta* **1999**, *292*, 172.
(23) (a) Patterson, T. A.; Carver, J. C.; Leyden, D. E.; Hercules, D. M. *J. Phys. Chem.* **1976**, *80*, 1700. (b) Wang, Y. C.; Li, F. Y.; Xu, L.; Jiang, N.; Liu, X. Z. *Dalton Trans.* **2013**, *42*, 5839.
(24) (a) Unoura, K.; Tanaka, N. *Inorg. Chem.* **1983**, *22*, 2963. (b) Fu, H.; Chen, W. L.; Wang, E. B.; Liu, J.; Chang, S. *Inorg. Chem. Acta* **2009**, *362*, 1412.
(25) (a) Martel, D.; Kuhn, A. *Electrochim. Acta* **2000**, *45*, 1829. (b) Ammam, M.; Mbomekalle, I. M.; Keita, B.; Nadjo, L.; Fransaer, J. *Electrochim. Acta* **2010**, *55*, 3118.
(26) Hao, N.; Shen, E. H.; Li, Y. G.; Wang, E. B.; Hu, C. W.; Xu, L. *Eur. J. Inorg. Chem.* **2004**, 4102.
(27) (a) Ley, K. D.; Schanze, K. S. *Coord. Chem. Rev.* **1998**, *171*, 287. (b) Yan, V. W. W.; Lo, K. K. W. *Chem. Soc. Rev.* **1999**, *28*, 323.
(28) (a) Dai, J. C.; Wu, X. T.; Fu, Z. Y.; Cui, C. P.; Hu, S. M.; Du, W. X.; Wu, L. M.; Zhang, H. H.; Sun, R. Q. *Inorg. Chem.* **2002**, *41*, 1391. (b) Zhang, L. Y.; Liu, G. F.; Zheng, S. L.; Ye, B. H.; Zhang, X. M.; Chen, X. M. *Eur. J. Inorg. Chem.* **2003**, *16*, 2965.
(29) Song, J. L.; Zhao, H. H.; Mao, J. G. *Chem. Mater.* **2004**, *16*, 1884.
(30) Qi, M. L.; Yu, K.; Su, Z. H.; Wang, C. X.; Wang, C. M.; Zhou, B. B.; Zhu, C. C. *Inorg. Chim. Acta* **2013**, *400*, 59.
(31) (a) Duncan, D. C.; Hill, C. L. *Inorg. Chem.* **1996**, *35*, 5828. (b) Dumas, E.; Debiemme-Chouvy, C.; Sevov, S. C. *J. Am. Chem. Soc.* **2002**, *124*, 908.
(32) Dumas, E.; Debiemme-Chouvy, C.; Sevov, S. C. *J. Am. Chem. Soc.* **2002**, *124*, 908.